PERGAMON

International Journal of Heat and Mass Transfer 42 (1999) 3585–3597

International Journal of HEAT and MASS TRANSFER

www.elsevier.com/locate/ijhmt

# Constructal trees of circular fins for conductive and convective heat transfer

A. Alebrahim, A. Bejan*

*Department of Mechanical Engineering and Materials Science, Box 90300, Duke University, Durham, NC 27708-0300, USA*

Received 25 August 1998; received in revised form 4 January 1999

**Abstract**

This paper extends to three dimensions and to convective heat transfer the constructal method of minimizing the thermal resistance between a volume and one point. In the first part of the paper, the heat flow mechanism is conduction, and the heat generating volume is occupied by low conductivity material ($k_0$) and high conductivity inserts ($k_p$). At the elemental-volume level the inserts are shaped as constant-thickness disks. In the first assembly the disks are mounted on a common stem of $k_p$ material. The internal and external geometric aspect ratios of the elemental volume and the first assembly are optimized numerically subject to volume constraints. In the second part of the paper the interstitial spaces once occupied by $k_0$ material are bathed by forced convection. The $k_p$ inserts function as 'fin material', and the first assembly becomes a fin bush with cylindrical symmetry. The geometry of the first assembly is optimized subject to total volume and solid volume constraints. The optimal number of circular fins, the optimal external shape of the assembly, the optimal ratio of the central stem diameter divided by the circular fin thickness, and the maximized global conductance of the assembly are reported as functions of the external flow (pressure drop number) and volume fraction of fin material. It is also shown that the optimization sequence can be shortened (albeit with approximate results) by adopting at the first-assembly level the internal geometric aspect ratios that were optimized independently at the elemental-volume level. © 1999 Elsevier Science Ltd. All rights reserved.

## 1. Objectives

The primary objective of this work is to extend to three-dimensional heat transfer the constructal method of minimizing geometrically the thermal resistance between a volume and one point. We pursue this objective by using volume elements and assemblies that possess cylindrical symmetry. This is an important step toward the optimization of real heat transfer devices, as the constructal method was originally based on the simplifying assumption that the flow of heat is two-dimensional [1,2]. The given volume generated heat at every point in a material with low thermal conductivity ($k_0$). A small amount of high thermal conductivity material ($k_p$) was distributed in the form of blade inserts through the $k_0$ medium.

The minimization of the overall volume-to-point thermal resistance consisted of 'constructing' the given volume in a sequence of building blocks that proceeds from the smallest size toward larger sizes (assemblies of smaller volumes). It is discovered that the shape of each block can be optimized such as its own volume-to-point resistance is minimal. The optimization continued with the optimal allocation of $k_p$ material to the high-conductivity blade of each building block. In the

* Corresponding author. Tel.: +1-919-660-5310; fax: +1-919-660-8963.

*E-mail address:* abejan@acpub.duke.edu (A. Bejan)

0017-9310/99/$ - see front matter © 1999 Elsevier Science Ltd. All rights reserved.
PII: S0017-9310(99)00021-6

**Nomenclature**

| | |
|---|---|
| $a$, $b$ | constants, Eqs. (19) and (21) |
| $A_c$ | cross sectional area |
| $c_p$ | fluid specific heat and constant pressure |
| $D_0$, $D_1$ | thicknesses of $k_p$ parts |
| $h_0$, $h_1$ | heat transfer coefficients |
| $\hat{h}$ | ratio of heat transfer coefficients, $h_1/h_0$ |
| $H_0$ | elemental length |
| $H_1$ | diameter |
| $k_0$ | low thermal conductivity |
| $k_p$ | high thermal conductivity |
| $\hat{k}$ | ratio of thermal conductivities, $k_p/k_0$ |
| $L_1$ | length |
| $m$ | parameter, Eq. (16) |
| $n_1$ | number of elemental volumes |
| $p$ | perimeter |
| $Pr$ | Prandtl number, $\nu/\alpha$ |
| $q_0$, $q_1$ | heat currents |
| $q'''$ | volumetric heat generation rate |
| $Re$ | Reynolds number, $U_\infty V_1^{1/3}/\nu$ |
| $T$ | solid temperature |
| $T_b$ | base temperature |
| $T_s$ | stem temperature |
| $T_\infty$ | free stream temperature |
| $U_\infty$ | free stream velocity |
| $V_0$, $V_1$ | volumes |
| $V_{p0}$, $V_{p1}$ | volumes filled by $k_p$ material |

*Greek symbols*

| | |
|---|---|
| $\alpha$ | fluid thermal diffusivity |
| $\Delta P$ | pressure difference |
| $\eta$ | fin efficiency |
| $\mu$ | viscosity |
| $\nu$ | kinematic viscosity |
| $\Pi$ | pressure drop number, Eq. (23) |
| $\rho$ | fluid density |
| $\phi_0$, $\phi_1$ | volume fractions occupied by $k_p$ material |

*Subscripts*

| | |
|---|---|
| mm | minimized twice |
| opt | optimum |
| peak | peak, largest value |
| 0 | elemental volume |
| 1 | first-assembly volume |

*Superscripts*

| | |
|---|---|
| $\tilde{(\ )}$ | dimensionless notation, Eqs. (3) and (4) |
| $\hat{(\ )}$ | dimensionless notation, Eqs. (10) and (11) |

end, the optimized path for volume-to-point heat flow emerged as a geometric structure in which every feature is deterministic. The high-conductivity paths formed a tree network, while the low-conductivity material filled the interstitial spaces contained between the smallest blades. Access to the infinity of points of the

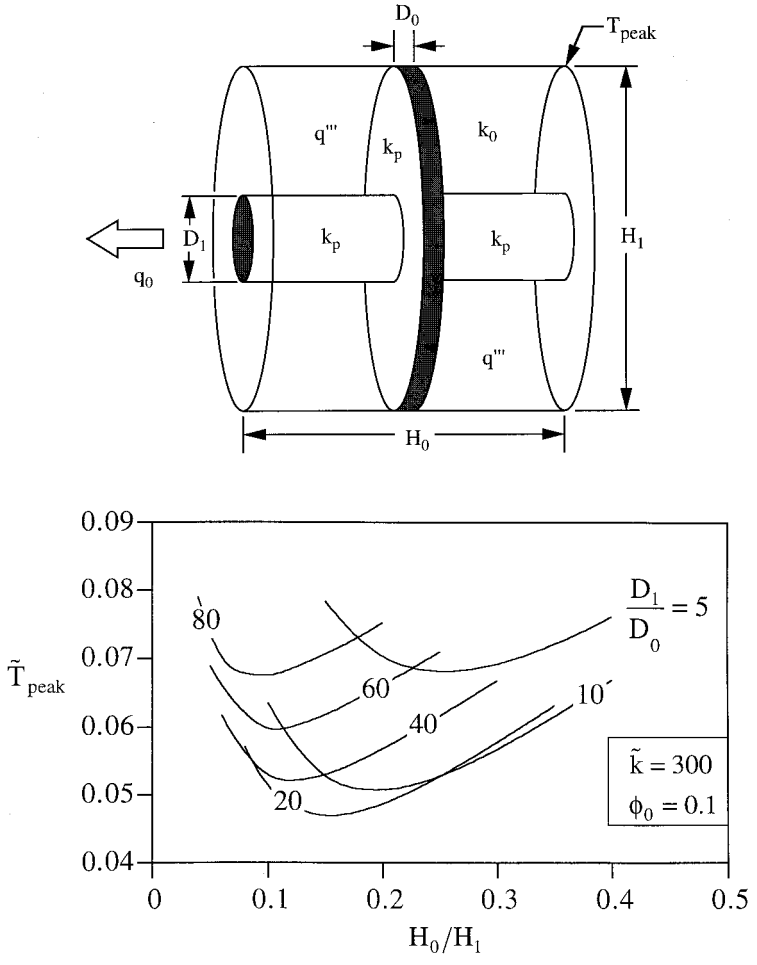


Fig. 1. Elemental volume for conduction in a heat-generating composite ($k_0$, $k_p$) with cylindrical symmetry, and the first optimization with respect to the external aspect ratio $H_0/H_1$.

heat-generating volume was made possible by the thermal diffusion through the $k_0$ material. The importance of the deterministic character of the volume-to-point flow structure and its generating principle was recognized in subsequent publications in the physics literature [3–7].

The second objective of the present work is to extend the minimization of volume-to-point resistance to conductive materials with compositions that depart from the asymptotic assumptions made in the earlier publications. Those assumptions were: (1) the ratio $k_p/k_0$ is much greater than 1, and (2) the volume fraction occupied by the $k_p$ material is much smaller than 1. In the present study the conductivity ratio and the volume fraction are two unspecified design parameters of the conductive composite.

The third objective is also the most novel and, potentially, the most useful. It is to take the constructal resistance-minimization method out of the field of conductive heat transfer and to apply it to its analog in convection: the optimization of the architecture of a tree of fins that connects with minimal resistance a boundary point (the fin root) to volume with convective fluid that is allocated to that point.

## 2. Conduction

### 2.1. Elemental volume

The geometric optimization work begins with dividing the given volume into building blocks of increasing sizes. The smallest such block is the 'elemental volume' shown in the upper part of Fig. 1. Most of this small volume is occupied by low-conductivity material ($k_0$) that generates heat at the uniform volumetric rate $q'''$. The volume is fixed,

Table 1
Comparison between the overall elemental-volume resistances calculated with the finite-elements and finite-differences codes

| $\tilde{k}$ | $\phi_0$ | $D_1/D_0$ | $H_0/H_1$ | $\tilde{T}_{peak}$(FE) | $\tilde{T}_{peak}$(FD) |
|---|---|---|---|---|---|
| 100 | 0.1 | 60 | 0.1 | 0.0946 | 0.0959 |
| 100 | 0.2 | 20 | 0.45 | 0.0703 | 0.0705 |
| 200 | 0.05 | 55 | 0.5 | 0.1295 | 0.1307 |
| 200 | 0.2 | 25 | 0.2 | 0.0280 | 0.0282 |
| 300 | 0.03 | 40 | 0.6 | 0.1525 | 0.1539 |
| 300 | 0.1 | 30 | 0.15 | 0.0367 | 0.0371 |
| 600 | 0.01 | 45 | 0.35 | 0.1872 | 0.1913 |
| 600 | 0.05 | 15 | 0.55 | 0.0865 | 0.0867 |
| 1000 | 0.01 | 50 | 0.3 | 0.1326 | 0.1354 |
| 1000 | 0.03 | 10 | 0.6 | 0.1023 | 0.1027 |

$$V_0 = \frac{\pi}{4} H_1^2 H_0 \tag{1}$$

but the geometric aspect ratio $H_0/H_1$ may vary. The generated heat current ($q_0$) is collected first by a disk-shaped insert of high thermal conductivity ($k_p$, $D_0$, $H_1$), and then taken out of the system through an axial stem ($k_p$, $D_1$, $H_0$). Heat is not being generated inside the $k_p$ material. The outer surface of the elemental volume $V_0$ is insulated, except over the heat-sink patch of diameter $D_1$, where the temperature is set equal to zero. The volume of the $k_p$ material allocated to the elemental volume is also constrained:

$$V_{p0} = \frac{\pi}{4}[D_1^2(H_0 - D_0) + H_1^2 D_0] \tag{2}$$

In accordance with the notation used in earlier constructal-theory papers, we express this constraint as the dimensionless volume fraction $\phi_0 = V_{p0}/V_0$.

In the steady state the temperature field established outside $V_0$ drives the total heat current toward the heat sink. We are interested in the magnitude and location of the peak temperature ($T_{peak}$), and in minimizing $T_{peak}$ by changing the geometry of the elemental volume. The peak temperature will occur along the ring of diameter $H_1$ that is situated the farthest from the heat sink.

The geometry of the elemental volume constrained by Eqs. (1) and (2) is represented by the external ratio $H_0/H_1$ and the internal ratio $D_1/D_0$. In principle, there is a third geometric parameter (a second internal ratio) that can be varied: the relative position of the $D_0$ disk on the $D_1$ stem of length $H_0$. We simplified this study by placing the $D_0$ disk in the midplane of the elemental volume, with the expectation that the ring of diameter $H_1$ that resides in the plane of the heat sink experiences a temperature comparable to, but somewhat lower than $T_{peak}$.

The equation for steady-state conduction with internal heat generation in cylindrical coordinates and the boundary conditions around $V_0$ are not listed here. We solved the conduction problem numerically by first defining the dimensionless variables

$$(\tilde{H}_0, \tilde{D}_0, \tilde{H}_1, \tilde{D}_1) = (H_0, D_0, H_1, D_1)/V_0^{1/3} \tag{3}$$

$$\tilde{T} = \frac{T}{q''' V_0^{2/3}/k_0} \tag{4}$$

such that the volume constraints (1) and (2) become

$$\tilde{H}_1^2 \tilde{H}_0 = \frac{4}{\pi} \tag{5}$$

$$\phi_0 = \frac{\pi}{4}[\tilde{D}_1^2(\tilde{H}_0 - \tilde{D}_0) + \tilde{H}_1^2 \tilde{D}_0] \tag{6}$$

The dimensionless version of the conduction equation and the interface conditions (the continuity of heat flux) between the $k_0$ and $k_p$ regions contains two dimensionless groups: $\phi_0$ and the conductivity ratio $\tilde{k} = k_p/k_0$.

The temperature field solution was determined by the finite element method. The code [8] was chosen because the optimization work required a reliable and flexible solver capable of generating efficiently a large number of simulations for many geometries. The method was based on quadrilateral elements with biquadratic interpolation function. The grid was uniform in the radial and axial directions, with 40 and 60 nodes, respectively. The fineness of this mesh was selected based on accuracy tests. For example, if the number of nodes is doubled in both the radial and axial directions, the dimensionless peak temperature changes by less than 0.5%.

The accuracy of the finite element method results (FE) was tested by comparing them with results based on our own finite difference code (FD). The smallest element was considered in the comparison. The discretized heat transfer equations were solved using Cholesky's method. The grid was uniform with 40

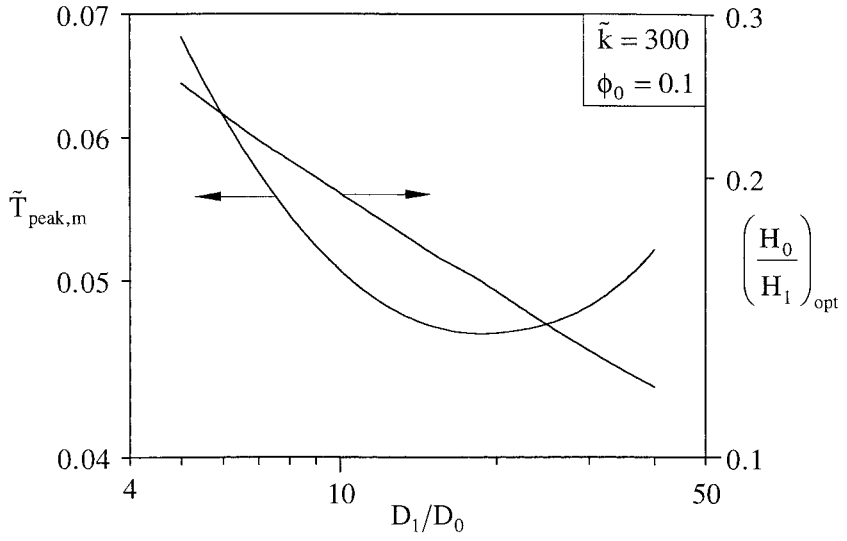


Fig. 2. The second optimization of the elemental volume with respect to the internal aspect ratio $D_1/D_0$.

nodes in the $r$-direction, and 60 nodes in the $z$-direction. Table 1 shows a comparison between the two sets of results (FE, FD) for the corner hot-spot temperature $\tilde{T}_{peak}$ at different values of $\tilde{k}$, $\phi_0$, $D_1/D_0$ and $H_0/H_1$. The agreement is consistently within 2.5%.

The numerical procedure consisted of fixing the geometrical configuration ($\tilde{k}$, $\phi_0$, $H_0/H_1$, $D_1/D_0$), calculating $\tilde{T}_{peak}$, and then changing the geometry in two ways ($H_0/H_1$ and $D_1/D_0$) in order to minimize $\tilde{T}_{peak}$. The double optimization sequence started with assuming a value for $D_1/D_0$ and minimizing $\tilde{T}_{peak}$ with respect to the external ratio $H_0/H_1$, as shown in the lower part of Fig. 1. In this step we used a version of constraint (5) that contained explicitly the external ratio: $\tilde{H}_0 = (4/\pi)^{1/3}(H_0/H_1)^{2/3}$. The results for the minimized peak temperature $\tilde{T}_{peak,m}$ and the optimal external ratio $(H_0/H_1)_{opt}$ are shown in Fig. 2.

In the second step we minimized $\tilde{T}_{peak,m}$ one more time by varying the internal ratio $D_1/D_0$. This step is illustrated in Fig. 2. The results are the twice-minimized peak temperature $\tilde{T}_{peak,mm}$, the optimal internal ratio $(D_1/D_0)_{opt}$ and the optimal external ratio $(H_0/H_1)_{opt}$ that corresponds to $(D_0/D_0)_{opt}$. These results are reported in Fig. 3, which also shows that the entire double-optimization was repeated for many property combinations of conductive composites ($\tilde{k}$, $\phi_0$). The data obtained for the twice-minimized peak temperature are correlated within 0.75% by the power law

$$\tilde{T}_{peak,mm} = 0.27\tilde{k}^{-0.67}\phi_0^{-0.88} \tag{7}$$

where it should be noted that $\tilde{T}_{peak,mm}$ also represents the twice-minimized thermal resistance between the elemental volume and its $D_1$-size boundary heat sink. The $\tilde{k}$ and $\phi_0$ effects revealed by Fig. 3 and Eq. (7) are comparable with the trends derived analytically for the two-dimensional elemental volume [1,2], where the twice-minimized thermal resistance was found to be proportional to $(\tilde{k}\phi_0)^{-1/2}$.

The influence of $\tilde{k}$ and $\phi_0$ on the optimal internal ratio is more interesting (Fig. 3, middle). When $\phi_0$ is greater than approximately 0.1, the ratio $(D_1/D_0)_{opt}$ increases monotonically as $\tilde{k}$ and $\phi_0$ increase. These trends are analogous to the results found for two-dimensional conduction (namely, Eq. (32) in Ref. [2]), where the optimal internal thickness ratio was equal to $(\tilde{k}\phi_0)^{1/2}$. When $\phi_0$ is considerably smaller than 0.1, the ratio $(D_1/D_0)_{opt}$ becomes less sensitive to changes in $\tilde{k}$, and when $\phi_0 = 0.01$ it decreases as $\tilde{k}$ increases.

The optimal external aspect ratio decreases as both $\tilde{k}$ and $\phi_0$ increase. The data reported in the bottom frame of Fig. 3 are correlated within 0.75% by

$$\left(\frac{H_0}{H_1}\right)_{opt} = 0.43\tilde{k}^{-0.39}\phi_0^{-0.51} \tag{8}$$

This behavior is almost the same as in the case of the two-dimensional elemental volume optimized in Ref. [2], in which the optimized external aspect ratio was shown to be equal to $2(\tilde{k}\phi_0)^{-1/2}$.

In summary, the geometrical form of the elemental volume of Fig. 1 can be optimized with respect to two degrees of freedom, the external ratio $H_0/H_1$ and the internal ratio $D_1/D_0$. The similarities between the results of this double optimization (Fig. 3) and the corresponding results for the two-dimensional elemental volume [1,2] strengthen our confidence in the present numerical work. These similarities indicate that the op-

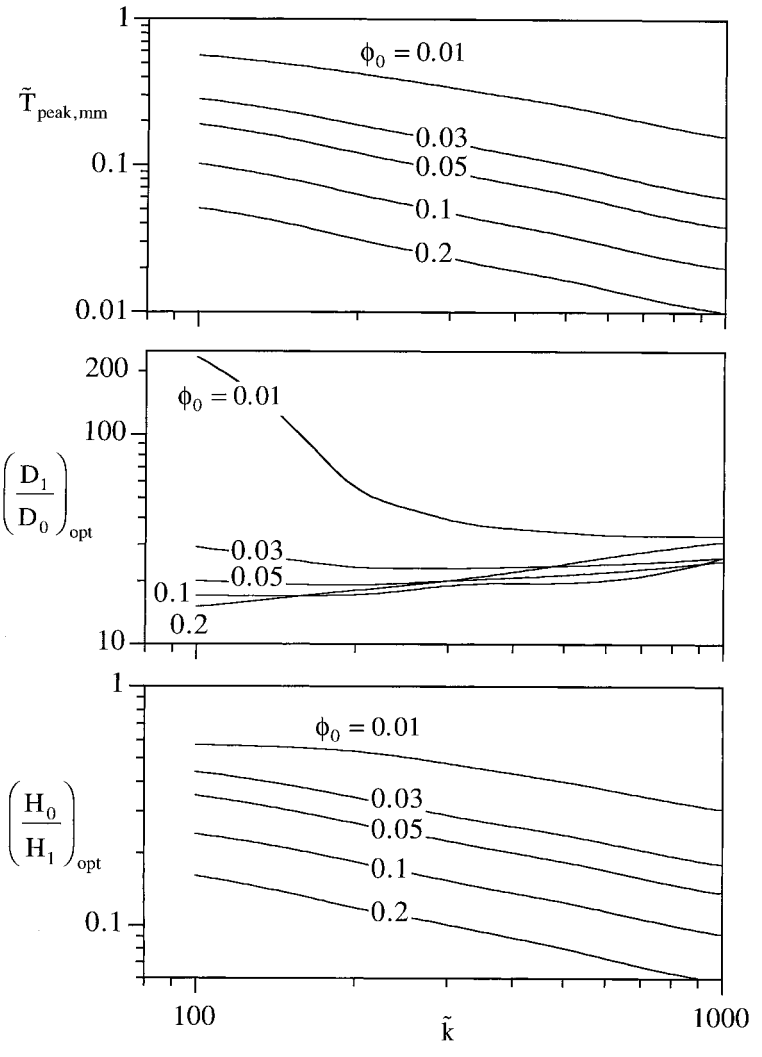


Fig. 3. The twice-minimized peak temperature, optimal internal aspect ratio, and optimal external aspect ratio of the elemental volume.

timal shapes at the elemental level are not influenced greatly by the two-dimensionality or three-dimensionality of the configuration.

The more practical conclusion that sends us in the direction pursued in the next section is that even in the twice optimized elemental volume the largest temperature difference will continue to increase proportionally with the size of the elemental volume [review the $\tilde{T}$ definition (4)]. Can this increase be slowed down by making additional changes in the geometrical form? The answer is 'yes': further improvements are possible if, in addition to the features optimized in this section, we increase the *internal complexity* of the given volume.

### 2.2. First assembly

Consider next the volume $V_1=(\pi/4)H_1^2L_1$ shown in the upper part of Fig. 4. To increase the complexity of this volume relative to that of Fig. 1, we took a number of ($n_1$) of elemental volumes and strung them up on a central stem of diameter $D_1$ and length $L_1$. In this way the structure of Fig. 4 becomes a 'first assembly' in the sense of constructal theory. The outer surface of the $V_1$ volume is insulated except over the axial spot of diameter $D_1$, which acts as heat sink ($T=0$). Fixed in the first assembly are the total volume $V_1$ and the volume of high-conductivity material,

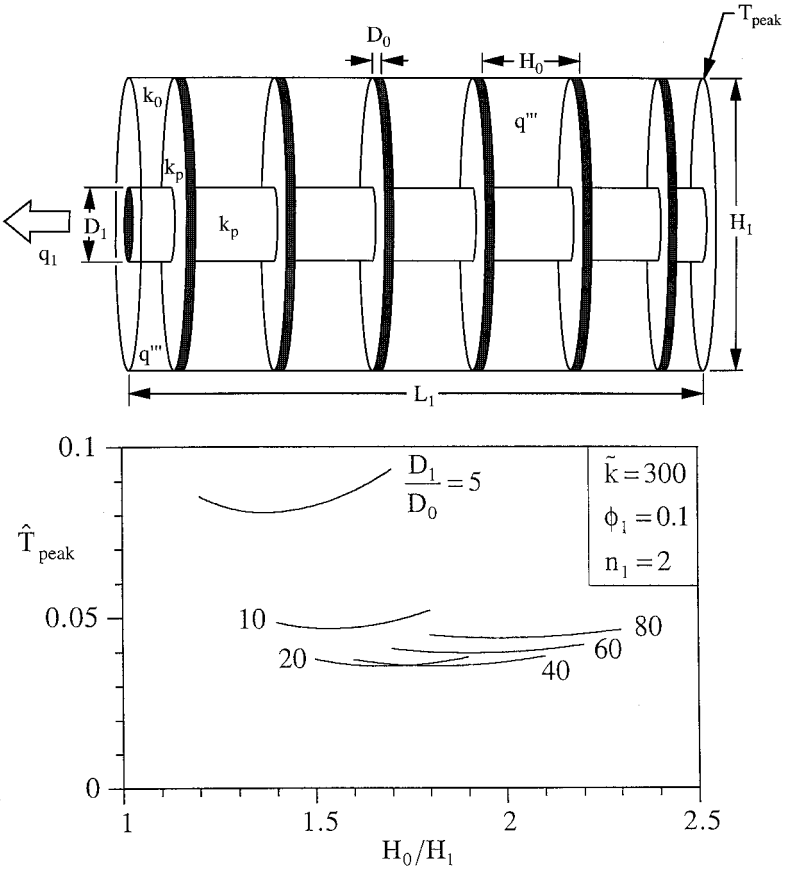


Fig. 4. The first assembly containing $n_1$ elemental systems cooled by the same central stem, and the optimization with respect to the aspect ratio $H_0/H_1$.

$$V_{p1} = n_1 \frac{\pi}{4} H_1^2 D_0 + n_1 \frac{\pi}{4} D_1^2 (H_0 - D_0) \tag{9}$$

The numerical formulation and procedure for determining the temperature field and $T_{peak}$ are the same as in section 2.1. As length scale we use $V_1^{1/3}$ such that the new dimensionless variables become

$$(\hat{H}_0, \hat{D}_0, \hat{H}_1, \hat{L}_1, \hat{D}_1) = (H_0, D_0, H_1, L_1, D_1)/V_1^{1/3} \tag{10}$$

$$\hat{T} = \frac{T}{q''' V_1^{2/3}/k_0} \tag{11}$$

The dimensionless $k_p$-volume constraint (9) assumes the form

$$\phi_1 = \frac{V_{p1}}{V_1} = \frac{\pi}{4}[n_1 \hat{H}_1^2 \hat{D}_0 + n_1 \hat{D}_1^2 (\hat{H}_0 - \hat{D}_0)] \tag{12}$$

The complete dimensionless formulation of the conduction problem in the volume $V_1$ (conduction equation, boundary conditions, and heat flux continuity between the $k_0$ and $k_p$ regions) depends on two dimensionless parameters of the composite medium: $\tilde{k}$ and $\phi_0$. These parameters are fixed during each act of geometric optimization.

The dimensionless peak temperature $\hat{T}_{peak}$ (see the upper right-hand corner of Fig. 4) depends on three dimensionless variables of the first-assembly geometry: the external aspect ratio $H_1/L_1$ and the internal ratios $H_0/H_1$ and $D_1/D_0$. Note that one of these variables (for example, $H_0/H_1$) can be replaced by the number $n_1$, because $n_1 = L_1/H_0$. The following results were developed by using $n_1$, $H_1/L_1$ and $D_1/D_0$ as variables. It is worth noting that when $n_1$ varies at constant $V_1$, the elemental volume surrounding a single $D_0$ disk (i.e., $V_0 = V_1/n_1$) varies.

To build on the numerical algorithm developed in Section 2.1, in the first assembly we began the optimization by fixing $n_1$ and minimizing $\hat{T}_{peak}$ twice, with respect to $H_0/H_1$ and $D_1/D_0$. This procedure is analogous to what we reported in Figs. 1 and 2, and is illustrated now for $n_1 = 2$ and $n_1 = 4$ in Figs 4 and 5.

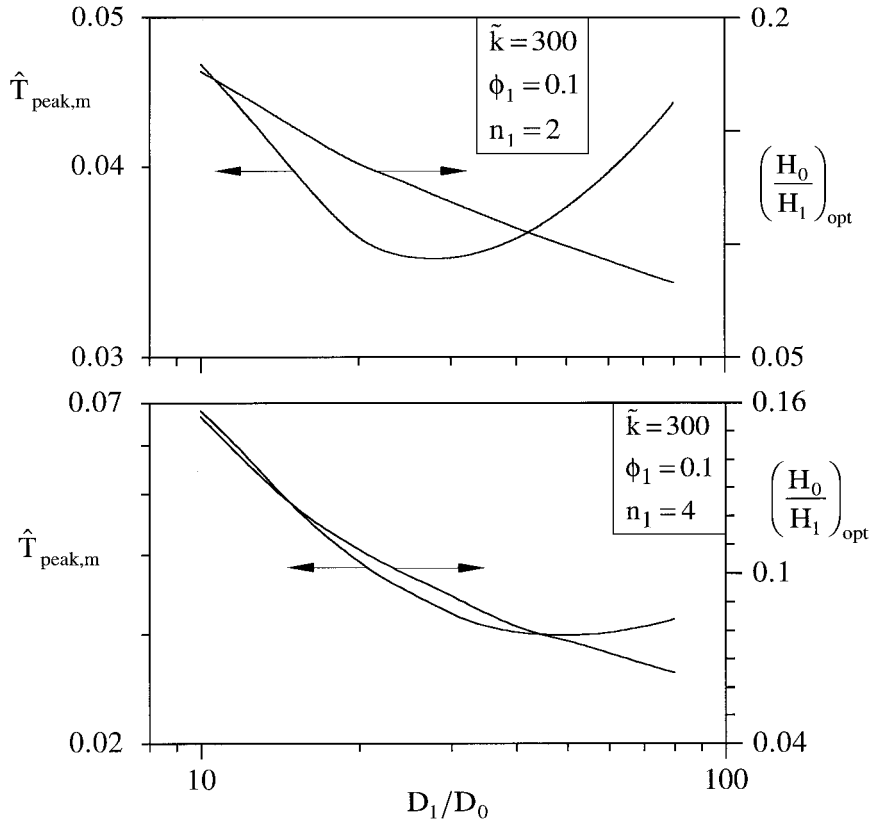


Fig. 5. The second optimization of the first assembly with respect to the internal aspect ratio $D_1/D_0$.

The twice minimized overall resistance and the optimized internal and external geometric ratios are reported in Fig. 6.

We repeated the double optimization procedure for higher $n_1$ values, in order to document the effect that the internal complexity has on the overall performance. The internal ratio $(D_1/D_0)_{opt}$ increases almost proportionally with $n_1$. The ratio $(H_0/H_1)_{opt}$ decreases monotonically as $n_1$ increases and, consequently, the corresponding external aspect ratio $(L_1/H_1)_{opt}$ is nearly constant. It can be verified that when $n_1 \geq 4$, the external ratio approaches $(L_1/H_1)_{opt} \cong 0.3$: this invariant of the optimized geometry is similar to the one encountered in two-dimensional trees for heat conduction [1–3]. The twice-minimized resistance of the assembly decreases monotonically as the number of elemental volumes increases.

We also varied the construction characteristics of the conductive composite in order to widen the $(\tilde{k}, \phi_0)$ domain of the design optimum. The results obtained for $(\tilde{k}=30, \phi_1=0.1)$ and $(\tilde{k}=300, \phi_1=0.01)$ have been projected on the same Fig. 6. The effects of $\tilde{k}$ and $\phi_0$ on $\hat{T}_{peak,mm}$ are expected: the overall resistance decreases when $\tilde{k}$ and $\phi_0$ increases. The internal and external aspect ratios $(D_1/D_0)_{opt}$ [and, correspondingly, $(L_1/H_1)_{opt}$] are relatively less sensitive to order-of-magnitude changes in both $\tilde{k}$ and $\phi_0$. These observations strengthen the invariant noted in the preceding paragraph. The optimized internal and external geometry is relatively *robust*, i.e., insensitive to small changes in material properties and amounts. We return to these properties of the optimized structure in Section 5.

## 3. Convection

The convection equivalent of the first assembly defined in Fig. 4 is the construct shown in the upper part of Fig. 7. The only solid is the $k_p$ material that fills the $D_0$ disks and the $D_1$ stem. Heat transfer occurs between the root disk $D_1$ and the fluid $(T_\infty)$ that flows along the faces of the $D_0$ disks. The total volume $[V_1=(\pi/4)H_1^2L_1]$ and the volume fraction occupied by the solid $(\phi_1=V_{p1}/V_1)$ are fixed. The number of $D_0$ fins installed on the stem is $n_1$. We seek to minimize the overall resistance by varying the external and internal geometric features of the assembly.

The overall resistance can be calculated in two steps.

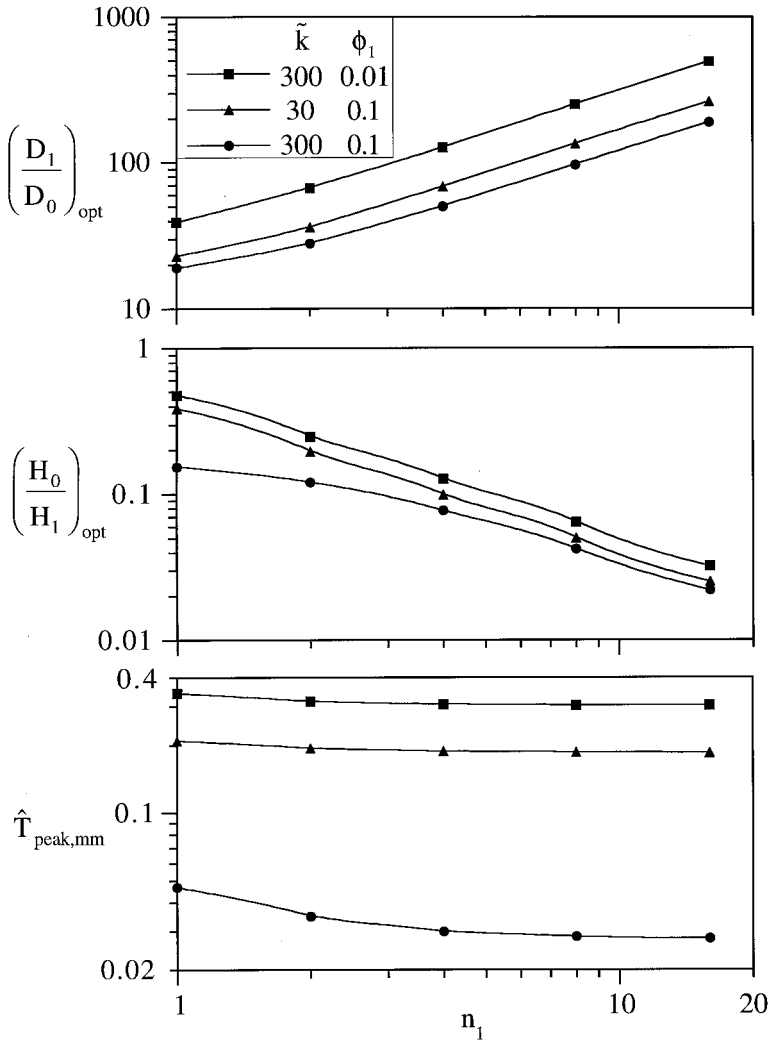


Fig. 6. The effect of the number of elemental volumes $n_1$ on the optimized geometry and performance of the first assembly.

First, we evaluate the heat transfer rate collected by the stem from each disk.

$$q_0 = \eta\frac{\pi}{2}(H_1^2 - D_1^2)h_0(T_s - T_\infty) \tag{13}$$

where the constant $h_0$ is the heat transfer coefficient on both sides of the $D_0$-thin plate. The fin efficiency $\eta$ is available in terms of Bessel functions [9], and is a function of two dimensionless parameters,

$$\eta = \text{function}\left[\left(\frac{H_1}{2} - \frac{D_1}{2}\right)\left(\frac{2h_0}{k_p D_0}\right)^{1/2}, \frac{H_1}{D_1}\right] \tag{14}$$

In the second step we average the $q_0$ effect of one circular fin over the stem surface of length $H_0$, which belongs to one fin. The heat flux $q_0/(\pi D_1/H_0)$ can be used to define an equivalent heat transfer coefficient $h_1$,

$$\frac{q_0}{\pi D_1 H_0} = h_1(T_s - T_\infty) \tag{15}$$

as if the stem, alone, were transferring heat to the flow. If we assume that the circular plate fins are sufficiently numerous and close to each other, then the $D_1$ stem performs as a one-dimensional fin with insulated end and uniform heat transfer coefficient $h_1$. The total heat transfer rate through the base ($T_b$) is given by the classical formula

$$q_1 = (T_b - T_\infty)(k_p A_c h_1 p)^{1/2} \tanh(mL_1) \tag{16}$$

where $A_c = (\pi/4)D_1^2$, $p = \pi D_1$ and $m = (h_1 p/k_p A_c)^{1/2}$. Eq. (16) can be nondimensionalized by using $V_1^{1/3}$ as length

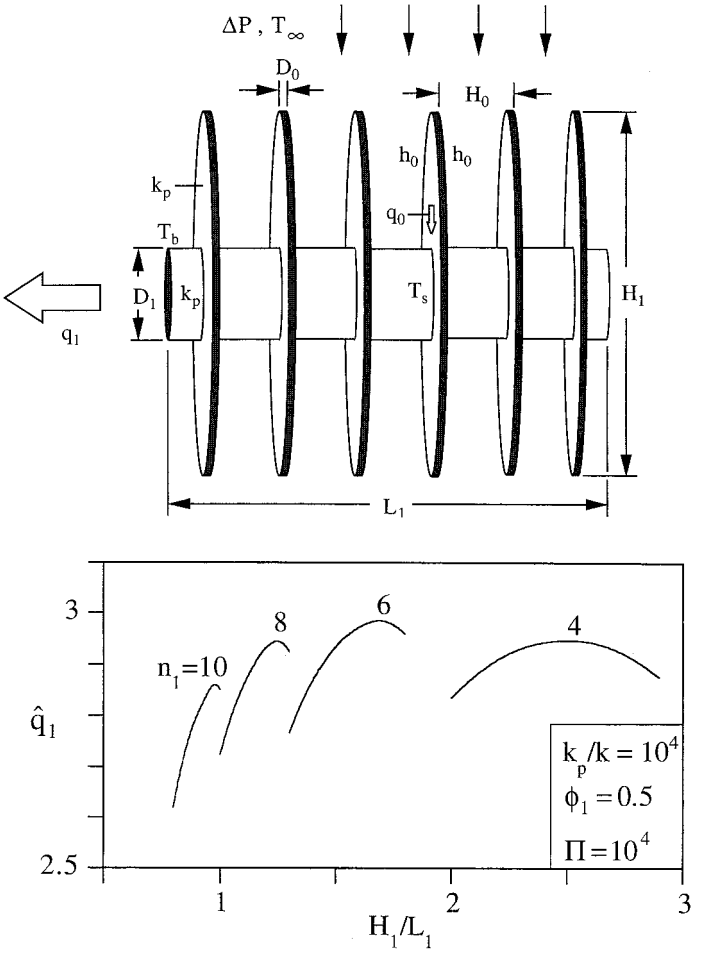


Fig. 7. First assembly with convective heat transfer in the interstices, and the double optimization of the geometric configuration.

scale (10) and $\hat{h}=h_1/h_0$. The resulting overall thermal conductance

$$\hat{q}_1 = \frac{q_1}{(T_b - T_\infty)(k_p V_1 h_0)^{1/2}} = \frac{\pi}{2}\hat{D}_1^{3/2}\hat{h}^{1/2}\ \tanh\left[2\hat{L}_1\left(\frac{\hat{h}}{\hat{D}_1}\right)^{1/2}\frac{h_0^{1/2}V_1^{1/6}}{k_p^{1/2}}\right] \tag{17}$$

shows the emergence of the dimensionless group $h_0^{1/2}V_1^{1/6}/k_p^{1/2}$. We seek an estimate for the heat transfer coefficient $h_0$, and note that it will vary with the dimensions of the spacing between two consecutive fins. In order to reduce the number of geometric degrees of freedom in the optimization of the $V_1$ assembly, we make the assumption that the shape of the space between consecutive fins has already been optimized for maximum conductance. Recent reviews on the geometric optimization of arrangements of electronics in constrained spaces have shown that in laminar forced convection the optimal spacing (in our case, $H_0 - D_0$) scales with the swept flow length ($H_1$) in the following proportion [10–13]

$$\frac{H_0 - D_0}{H_1} \sim \left(\frac{\mu\alpha}{H_1^2\Delta P}\right)^{1/4} \tag{18}$$

The pressure difference $\Delta P$ is maintained by a fan in order to drive the flow through the assembly of Fig. 7. Nondimensionalized, Eq. (18) becomes

$$\frac{\hat{H}_0 - \hat{D}_1}{\hat{H}_1^{1/2}} = a \tag{19}$$

where $a=(\mu\alpha/V_1^{2/3}\Delta P)^{1/4}$ is a dimensionless parameter. This optimal-interstice design is characterized by a maximum conductance [10,11] that can be rewritten as an estimate for the order of magnitude of the inter-

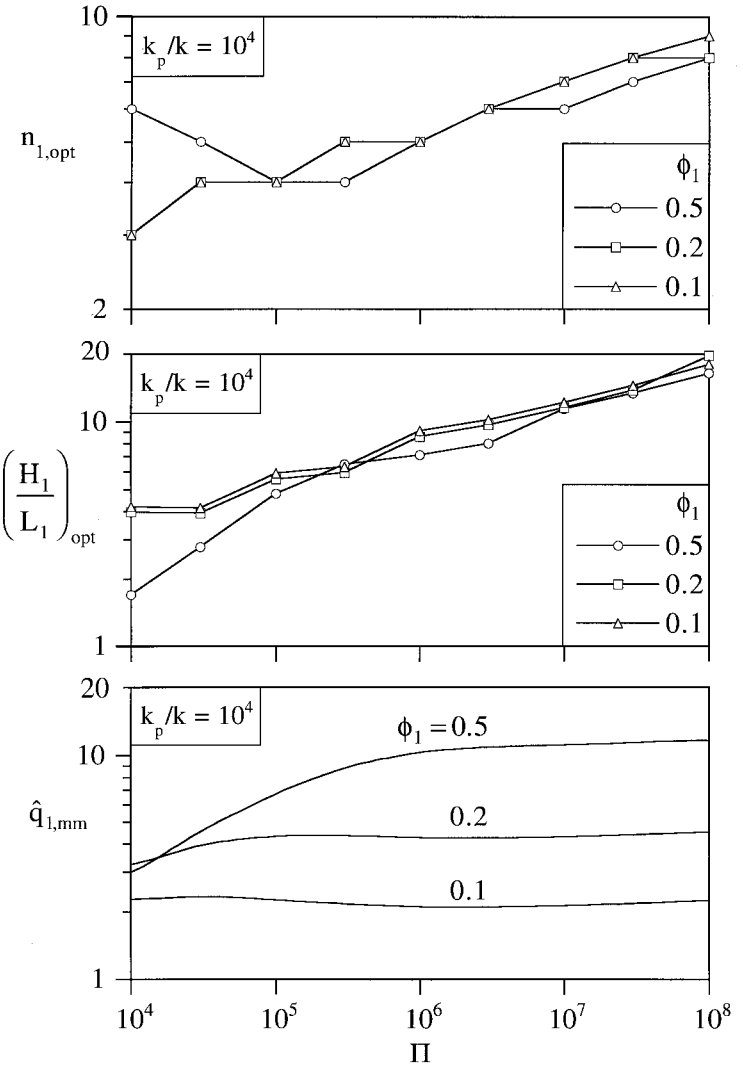


Fig. 8. The number of elemental volumes, optimal external aspect ratio, and twice-maximized conductance of the first assembly with convective heat transfer.

stitial heat transfer coefficient:

$$h_0 \sim \left(\frac{\rho \Delta P}{Pr}\right)^{1/2} c_p \tag{20}$$

In this way the heat transfer coefficient $h_0$ emerges as a constant set by the fan ($\Delta P$), which is why $h_0$ is used as a constant in the definitions of $\hat{q}_1$ and $\hat{h}$. The dimensionless group revealed by Eq. (17) assumes the form

$$\frac{h_0^{1/2} V_1^{1/6}}{k_p^{1/2}} = b \tag{21}$$

where $b = [(c_p V_1^{1/3}/k_p)(\rho \Delta P/Pr)^{1/2}]^{1/2}$ is another parameter. It can be shown that parameters $a$ and $b$ are related through the pressure drop number $\Pi$,

$$a = \Pi^{-1/4}, \quad b = \left(\frac{k}{k_p}\right)^{1/2} \Pi^{1/4} \tag{22}$$

where the pressure drop number is defined as [11,12]

$$\Pi = \frac{\Delta P V_1^{2/3}}{\mu \alpha} \tag{23}$$

The rest of the problem statement can be put in the same nondimensional notation as Eq. (17). Eqs. (13) and (15) provide the needed expression for $\hat{h}$,

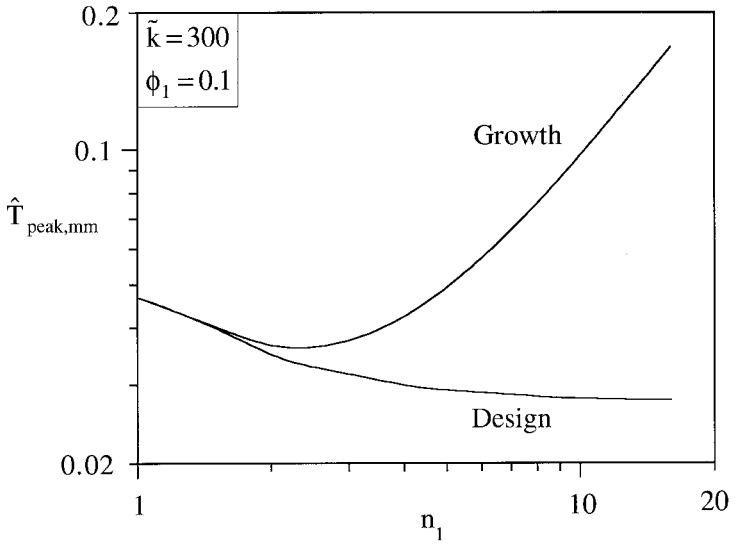


Fig. 9. The twice-minimized overall resistance of the conductive first assemblies optimized using the design method and the growth method.

$$\hat{h}=\frac{2\eta}{\hat{D}_1\hat{H}_0}(\hat{H}_1^2-\hat{D}_1^2) \tag{24}$$

The fin efficiency (14) assumes the dimensionless form

$$\eta=\text{function}[(\hat{H}_1-\hat{D}_1)b/(2\hat{D}_0)^{1/2},\ \hat{H}_1/\hat{D}_1] \tag{25}$$

The geometric relations are the total-volume constraint, the solid-fraction volume constraint, and the number of circular plate fins,

$$\hat{H}_1^2\hat{L}_1=4/\pi \tag{26}$$

$$\phi_1=n_1\frac{\pi}{4}(\hat{H}_1^2-\hat{D}_1^2)\hat{D}_0+\frac{\pi}{4}\hat{D}_1^2\hat{L}_1 \tag{27}$$

$$n_1=\hat{L}_1/\hat{H}_0 \tag{28}$$

In summary, there are seven equations [namely, (17), (19), (24)–(28)] that contain nine dimensionless variables, $\hat{H}_1$, $\hat{D}_1$, $\hat{L}_1$, $\hat{H}_0$, $\hat{D}_0$, $n_1$, $\hat{q}_1$, $\hat{h}$ and $\eta$. The design has two degrees of freedom, one external and the other internal, namely $H_1/L_1$ and $n_1$, or $H_1L_1$ and $D_1/D_0$. The physical parameters $\phi_1$, $\Pi$, and $k_p/k$ are fixed, and play the role of constraints. The objective is to maximize $\hat{q}_1$ in two dimensions subject to the constraints. This procedure is illustrated for one case in the lower part of Fig. 7, where it is found that the best geometry is represented by $n_{1,\text{opt}}=6$ and $(H_1/L_1)_{\text{opt}}=1.696$.

We repeated this double optimization for other combinations of solid volume fraction $\phi_1$ and pressure drop number $\Pi$. All this work was conducted by setting $k_p/k=10^4$, which is the correct order of magnitude for the combination of copper in the solid part and room air in the fluid part. The results are presented in Fig. 8. The twice maximized conductance $\hat{q}_{1,\text{mm}}$ increases monotonically with both $\phi_1$ and $\Pi$, which is the expected trend. The optimal number of elements increases slowly as $\Pi$ increases: this trend is almost insensitive to $\phi_1$ when $\phi_1$ is of the order of 0.1 or smaller. The external aspect ratio $(H_1/L_1)_{\text{opt}}$ is more sensitive to changes in $\Pi$ because the interstitial spaces $H_0$ become narrower as $\Pi$ increases [cf. Eq. (18)].

The body of work on the geometric optimization of electronic packages [13] shows that the effect of the pressure drop number $\Pi$ can be expressed more readily in terms of the free stream velocity of the stream. The order of magnitude of $\Delta P$ is $\rho U_\infty^2$ and this transforms the definition (22) into

$$\Pi\cong Re^2Pr \tag{29}$$

where $Re=U_\infty V_1^{1/3}/\nu$ and $Pr=\nu/\alpha$. The pressure drop number accounts for the free stream velocity squared.

## 4. The 'design' method vs the 'growth' method

All the optimization work performed for the first assembly with internal conduction (Section 2.2) and internal convection (Section 3) was one of 'designing' the interior of a volume ($V_1$) that is fixed. All the geometric features —internal and external—were allowed to vary freely during the design. We refer to this approach of working 'inward' as the 'design method'.

A more direct alternative is to proceed 'outward'

and to build—to grow—the volume $V_1$ from an appropriate number of *optimized* elemental volumes [1,2]. We refer to this approach as the 'growth method'. In this case the aspect ratios of the elemental volume ($D_1/D_0$, $H_0/H_1$) are taken from the elemental results of section 2.1 (Fig. 3), and are no longer free to vary in the optimization of the first assembly. The advantage of the growth method is that the number of degrees of freedom at the first-assembly level is smaller, which is why the growth method is more direct and computationally less expensive.

How accurate is the growth method in relation to the more rigorous design method? In Fig. 9 we show the minimized overall resistance of a first assembly ($\tilde{k}=300$, $\phi_1=0.1$) optimized using the two methods. The result produced by the design method is the same as the $\hat{T}_{\text{peak,mm}}$ curve shown in Fig. 6: the global resistance decreases monotonically as $n_1$ increases, however, diminishing returns are registered with $n_1$ becomes greater than 4. The curve for the growth method was generated for the same volume $V_1$ by fixing $n_1$ and using in the first-assembly design the $(D_1/D_0)_{\text{opt}}$ and $(H_0/H_1)_{\text{opt}}$ ratios read from Fig. 3 for $\tilde{k}=300$. We learn from Fig. 9 that according to the growth method there is an optimal number of elements ($n_1$), whereas in the design method the overall resistance decreases monotonically as $n_1$ increases. The minimum of the growth curve occurs at an $n_1$ value that can also be associated with the point of diminishing returns that is reached along the design curve.

In conclusion, the growth method can be used as shortcut to designs that approach the performance of the truly optimal configuration that is generated by the design method. The configuration produced by the growth method can be refined later based on the design method. It can also be used as first guess in optimization routines based on the design method. That the 'growth' and the 'design' configurations perform similarly even though their internal geometries differ is an indication that when the structure is sufficiently complex, the internal details play a minor role in the global performance of the optimized flow system. The same conclusion was reached in two-dimensional point-to-volume flows [2,3], and is an important feature in natural flow structures. Several other similarities between the present three-dimensional structures and the two-dimensional trees were signaled at various stages in the main body of this paper.

Unlike in two-dimensional systems, the present optimization sequence cannot be extended routinely to assemblies of higher order, because of the cylindrical symmetry adopted for the elemental system and the first assembly. A second assembly could be formed by mounting two or more first assemblies on a new central stem of diameter $D_2$ and length $L_2$, like buds or pine cones on a branch. The structure of such an assembly will not fill its allotted volume completely.

## Acknowledgements

This research was sponsored by the National Science Foundation (USA) and Kuwait University.

## References

[1] A. Bejan, Advanced Engineering Thermodynamics, Wiley, New York, 1997.
[2] A. Bejan, Constructal-theory network of conducting paths for cooling a heat generating volume, International Journal of Heat and Mass Transfer 40 (1997) 799–816.
[3] G.A. Ledezma, A. Bejan, M.R. Errera, Constructal tree networks for heat transfer, Journal of Applied Physics 82 (1997) 89–100.
[4] A. Bejan, M.R. Errera, Deterministic tree networks of fluid flow: geometry for minimum flow resistance between a volume and one point, Fractals 5 (1997) 685–695.
[5] A. Bejan, G.A. Ledezma, Streets tree networks and urban growth: optimal geometry for quickest access between a finite-size volume and one point, Physica A 255 (1998) 211–217.
[6] N. Dan, A. Bejan, Constructal tree networks for the time-dependent discharge of a finite-size volume to one point, Journal of Applied Physics 84 (1998) 3042–3050.
[7] M.R. Errera, A. Bejan, Deterministic tree networks for river drainage basins, Fractals 6 (1998) 245–261.
[8] FIDAP Theory Manual, V.7.0, Fluid Dynamics International, Evanston, IL 1993.
[9] H.S. Carslaw, J.C. Jaeger, Conduction of Heat in Solids, Oxford University Press, Oxford, UK, 1959.
[10] A. Bejan, E. Sciubba, The optimal spacing of parallel plates cooled by forced convection, International Journal of Heat and Mass Transfer 35 (1992) 3259–3264.
[11] A. Bejan, Convection Heat Transfer, Wiley, New York, 1995.
[12] S. Petrescu, Comments on the optimal spacing of parallel plates cooled by forced convection, International Journal of Heat and Mass Transfer 37 (1994) 1283.
[13] S.J. Kim, S.W. Lee, Air Cooling Technology for Electronic Equipment, CRC Press, Boca Raton, FL, 1995 chap. 1.